Korean J. Chem. Eng., 33(6), 1942-1947 (2016)
DOI: 10.1007/s11814-016-0035-4

pISSN: 0256-1115
eISSN: 1975-7220

Crystal growth of ionic semiclathrate hydrate formed at interface between CO_2+N_2 gas mixture and tetrabutylammonium bromide aqueous solution

Hiroaki Hayama, Hotaka Akiba, Yuki Asami, and Ryo Ohmura†

Department of Mechanical Engineering, Keio University, 3-14-1 Hiyoshi, Kohoku-ku, Yokohama 223-8522, Japan
(*Received 30 October 2015 • accepted 30 January 2016*)

Abstract−This study reports a visual observation of the formation and growth of ionic semiclathrate hydrate on the surface of a Tetrabutylammonium bromide (TBAB) aqueous solution and CO_2+N_2 gas mixture. The composition of CO_2+N_2 gas mixture was 20 : 80. The experimental temperature range was from 280 K to 290 K, under the pressures of 2.3 MPa and 4.7 MPa, at w_{TBAB}=0.10 and w_{TBAB}=0.40, where w_{TBAB} denotes the mass fraction of TBAB in the aqueous solution. At w_{TBAB}=0.40, the hydrate crystals were initially observed to grow within the droplet, and followed by lateral growth at the droplet surface; but at w_{TBAB}=0.10, the hydrate crystals grew exclusively in the liquid phase and did not cover the droplet surface. Two types of different crystals with different sizes were clearly observed.

Keywords: Clathrate Hydrate, Crystal Growth, Carbon Capture, Crystal Morphology, Tetrabutylammonium Bromide

INTRODUCTION

In 2014, the Intergovernmental Panel on Climate Change (IPCC) reported that carbon dioxide (CO_2) emissions should be ceased by 2100 in order to prevent a 2 K global temperature rise from the 19th century [1]. As one method to reduce carbon dioxide emission, carbon capture and storage (CCS) technology has garnered wide attention. CCS technology is mainly applied to flue gas from thermal power plants and steelworks. The main components of flue gas are CO_2 and nitrogen (N_2) which mainly have a composition of CO_2 : N_2=20 : 80. Despite its small fraction, CO_2 gas released from these sources is still detrimental to the environment, and therefore should be separated and captured. It is important for the CCS technology to have a small environmental load and low cost than existing CO_2 separation and capture technology. Carbon capture using clathrate hydrate is one such technology [2].

Clathrate hydrates (hereafter hydrates) are crystalline solids composed of hydrogen-bonded cage-forming water molecules called the "host" and enclose different molecules called "guests" within those cages. Hydrates are usually stable at low temperature and high pressure conditions. It is generally known that hydrates have several properties, such as high gas-storage capacity, large heat of formation and decomposition, and guest substance selectivity. These properties enable hydrates to be applied to various industrial technologies, for example, transportation and storage of natural gas and hydrogen [3-6], the ocean and ground sequestration of CO_2 [7-9], developing highly efficient heat pump and refrigeration [10], and gas separation [2].

Hydrate selectivity in enclosing guest molecules differs depending on the guest species. For flue gas, CO_2 is preferentially enclosed in the hydrate cages in comparison to N_2. Taking this phenomenon as an advantage, various CO_2 capture methods using hydrates are proposed by Huen Lee and coworkers [2,11,12]. To improve the efficiency of their design, in this study, we acknowledge that the need for a more comprehensive understanding of hydrate growth behavior and hydrate crystal morphology is important. Here, hydrate crystal morphology denotes the crystal size and shape. Within their proposal, a hydrate utilizing CO_2 capture technology is composed of several processes including hydrate formation, hydrates and water transportation, dehydration, and hydrates decomposition. The hydrate transportation process means transferring hydrates and its slurry to a subsequent process through pipelines. Hydrate slurry is reported to show a similar behavior to Bingham fluid. Therefore, larger crystals and low viscous hydrate slurry are preferred as they use up as a smaller amount of energy in this process [13]. The dehydration process means separating hydrates from its aqueous solution to dissolve hydrates. If crystals are bigger, the dehydration process achieves higher efficiency [14]. The decomposition process means to dissociate hydrate into water and guests. Large hydrate crystals have small specific surface areas, which reduces the overall rate of heat transfer. From the above, it is important to consider the hydrate morphology for designing efficient transportation, dehydration and decomposition processes.

One of the methods to alleviate the low temperature and high pressure formation conditions is adding ionic guest substance to water, which will cause guests to form ionic semiclathrate hydrates. Slightly differing from canonical clathrate hydrates, ionic semiclathrate hydrates' structure has anions substituted to be a part of the cage structures resulting in water molecules and cations incorporated cage. Tetrabutylammonium bromide (TBAB) is a low cost and environmentally friendly ionic guest. The TBAB semiclathrate hydrates have empty cages which are available to enclose small guest substance, e.g., H_2, CO_2, and CH_4 and have been used for gas separation [15-17]. Therefore, CO_2 separation from flue gas using TBAB semiclathrate hydrate has been successfully demonstrated [18,19]. The hydrate formation equilibrium temperature of a sys-

†To whom correspondence should be addressed.
E-mail: rohmura@mech.keio.ac.jp

tem including CO_2+N_2 (mass fraction CO_2 : N_2=20 : 80) and TBAB (w_{TBAB}=0.40) system 20 K higher than that of CO_2+N_2 system at the same pressure, 4.7 MPa [20,21], where w_{TBAB} denotes the mass fraction of TBAB in the aqueous solution.

Oyama et al. [22] observed the crystals of TBAB hydrates in TBAB aqueous solution at atmospheric pressure. The two different geometric shapes of TBAB hydrates crystals were observed at w_{TBAB}=0.357. They inferred that the crystals structure depended on hydration number; for example, one had a hydrate number of 38 formed an undefined shape composed of thin crystals, while the other which had a hydration number of 26 formed columnar shaped crystals. Veluswamy et al. [23] reported the morphology of hydrogen+TBAB semiclathrate hydrates. They confirmed that the difference of TBAB concentration affected the crystal morphology. At w_{TBAB}=0.15 and w_{TBAB}=0.27, they initially formed equiaxial crystals and needle-like crystals which later developed into columnar crystals. At w_{TBAB}=0.31, w_{TBAB}=0.36, w_{TBAB}=0.41, the cylinder like crystals that formed at first were observed to develop into dense irregular shaped crystals. Koyanagi and Ohmura [24] observed CO_2+TBAB hydrates in TBAB aqueous solution system to understand the hydrate growth in the liquid phase at w_{TBAB}=0.10 and w_{TBAB}=0.40 at 2.3 or 3.4 MPa. In this case, the hydrate growth behavior did not depend on the pressure and TBAB mass fraction. The morphology of CO_2+TBAB hydrate was replaced from the wedge crystals to polygonal columnar, needle and sword-like crystals. Akiba et al. [25] reported the semiclathrate hydrates formed of CO_2+TBAB aqueous droplet system to understand the hydrate growth at the gas/liquid interface at w_{TBAB}=0.10 and w_{TBAB}=0.40, at 2.3 MPa. The observation of hydrates crystals growing inside a droplet of TBAB aqueous solution is unique as most hydrates grow at liquid/gas interface. They observed two types of the crystal morphology. One was step-shaped crystals, the other was polygonal-shaped crystals. Because in both previous studies [24,25] the nucleation occurred at gas/liquid interface, it is important to observe the crystal growth at gas/ liquid interface.

To utilize hydrates for CO_2 capture technology, it is necessary to observe hydrate crystals at the same composition as flue gas. In this study, we report visual observations of hydrate growth behavior and crystal morphology at the interface between CO_2+N_2 gas mixture and TBAB aqueous solution.

EXPERIMENTAL SECTION

A gas mixture of CO_2 and N_2 with a composition of CO_2 : N_2= 20 : 80 (Taiyo Nippon Sanso Co.) was used in this experiment. TBAB aqueous solution was prepared by dissolving TBAB of solid reagent (99.0 mass%, Aldrich Chemical Co.) into distilled water and set for two different concentrations, w_{TBAB}=0.10 and w_{TBAB}=0.40. w_{TBAB}=0.40 was the congruent composition [30,31] and at w_{TBAB}= 0.10 the process using hydrates becomes efficient because the hydrates can be treated as the hydrate slurry. The crystals have the possibility to form the different crystals of the hydration number. For the above reasons, we settled on these two different concentrations.

In this study, we used essentially the same experimental apparatus and experimental procedure as Akiba et al. Fig. 1 shows the

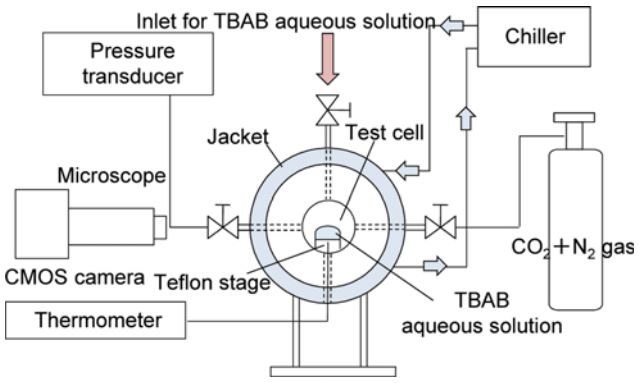

Fig. 1. Schematic diagram of the experimental apparatus.

schematic diagram of the experimental apparatus used in this study. The test cell is a cylindrical vessel made of stainless steel. The inner space of the test cell functions to hold the test gas and hydrate crystals is 25 mm in diameter and 20 mm in axial length. Test cell temperature is controlled by circulating ethylene glycol aqueous solution in the jacket covering the test cell. A droplet of TBAB aqueous solution was placed on the Teflon stage in the test section. The air was then replaced with the gas mixture of CO_2 and N_2 from the gas cylinder to the test cell valve by repeating the pressurization and depressurization of the cell with the gas mixture. The pressure of inside the test cell, P was measured by a strain gauge pressure sensor with an uncertainty of ±0.02 MPa. The droplet temperature on the Teflon stage, T, was measured by Pt-resistance thermometer with an uncertainty of ±0.2 K inserted just below the Teflon stage. As a precaution, it was confirmed that the temperature of the droplet and Teflon stage was equal by measuring the droplet temperature with the inserting Pt-resistance thermometer into the droplet, then the thermometer was removed.

Equilibrium temperature, T_{eq} of CO_2+N_2+TBAB hydrates for the prescribed pressure (2.3 MPa or 4.7 MPa) and TBAB concentration (w_{TBAB}=0.10 or w_{TBAB}=0.40) were experimentally determined prior to the observational experiments. CO_2 and N_2 gas mixture were supplied to the test cell up till the prescribed pressure. T was set to the equilibrium temperature of TBAB simple hydrates. The system temperature T was increased stepwise by 0.1 K. At each step, if no remarkable change of hydrates dissociation was observed within 1 h, the system temperature T was increased. The temperature at which the hydrates were visually observed to have dissociated completely was determined to be the equilibrium temperature, T_{eq}. By repeating this procedure of visual observation and stepwise temperature increase, the equilibrium temperature of CO_2+N_2+TBAB hydrates was determined. The equilibrium temperature measurements were performed for each TBAB concentrations and pres-

Table 1. Equilibrium condition of CO_2+N_2+TBAB hydrates

w_{TBAB}	P/MPa	T_{eq}/K
0.10	2.3	283.7
	4.7	286.3
0.40	2.3	287.6
	4.7	289.0

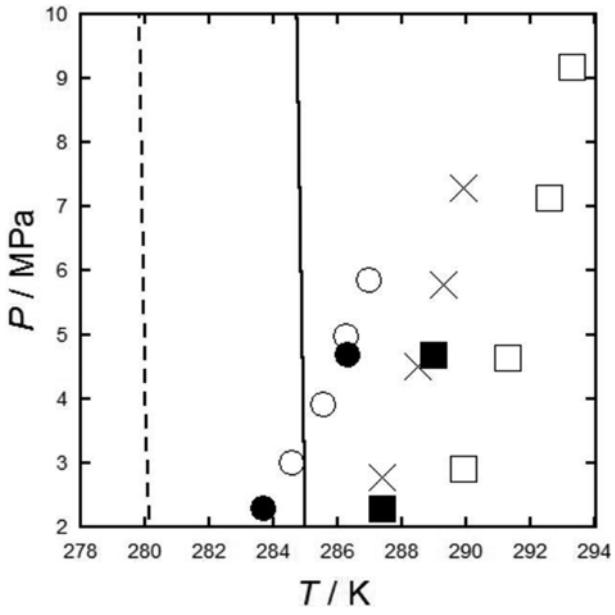

Fig. 2. Equilibrium conditions of TBAB simple hydrates and CO_2+N_2+TBAB hydrates. —: TBAB simple hydrates (w_{TBAB}=0.40) [26], - -: TBAB simple hydrates (w_{TBAB}=0.10) [27], □: CO_2+N_2+TBAB hydrates (w_{TBAB}=0.40) (CO_2 : N_2=15 : 75) [21], ○: CO_2+N_2+TBAB hydrates (w_{TBAB}=0.10) (CO_2 : N_2=20 : 80) [28], ×: CO_2+N_2+TBAB hydrates (w_{TBAB}=0.407) (CO_2 : N_2=20 : 80) [29], ■: CO_2+N_2+TBAB hydrates (w_{TBAB}=0.40) (CO_2 : N_2= 20 : 80) (this study), ●: CO_2+N_2+TBAB hydrates (w_{TBAB}=0.10) (CO_2 : N_2=20 : 80) (this study).

sures. We show the measured equilibrium conditions in Table 1 and phase diagram in Fig. 2.

In the observational experiment of crystal growth and morphology, initially, the pressure was set to 2.3 MPa or 4.7 MPa and the temperature of the Teflon stage was decreased to about 270 K to form CO_2+N_2+TBAB hydrates, TBAB semiclathrate hydrate and ice. Then, T was increased to 0.5 K higher than T_{eq}. We applied the memory effect to shorten induction time for hydrate nucleation. After visually confirming that the all hydrate crystals were dissociated, we decreased T to set the prescribed subcooling ΔT_{sub}. We defined the subcooling, ΔT_{sub}, the difference between the system temperature and the equilibrium temperature of CO_2+N_2+TBAB hydrates ($\Delta T_{sub} \equiv T_{eq} - T_{ex}$), as driving force index for crystal growth. We conducted the experiments above equilibrium temperature of TBAB simple hydrates and for several different subcooling ΔT_{sub} in the range from 2 K to 4 K. We monitored and recorded the crystal growth of the hydrates using a CMOS camera (CMOS300-USB2, Fortissimo Co.) and a microscope (VZMis450i, Edmund optics).

RESULTS AND DISCUSSION

Sequential images of representative CO_2+N_2+TBAB hydrate growing processes at w_{TBAB}=0.40 and w_{TBAB}=0.10 are shown in Figs. 3 and 4. We defined the time when the first hydrate crystal was visually confirmed as t=0. The elapsed time is shown below each image. The right side images in Figs. 3 and 4 show the hydrate crystals that have just stopped their growth. It was confirmed that the hydrate crystals did not change after leaving it for 3 h. At w_{TBAB}= 0.40, the hydrate crystals were observed initially to grow within the droplet (liquid phase) (Fig. 3 central image). It was then followed by lateral growth at the surface (gas/liquid interface) (Fig. 3 right image). In contrast at w_{TBAB}=0.10, the hydrate crystals grew exclusively in the liquid phase and did not cover the CO_2+N_2 gas/TBAB aqueous solution interface. Note that the curved surface of the droplet was maintained at w_{TBAB}=0.10 (Fig. 4 right image), whereas the droplet surface was covered by polycrystalline layer at w_{TBAB}=0.40 (Fig. 3 right image). From this observation, it is found that the hydrate crystals did not cover the gas/liquid interface at w_{TBAB}=0.10.

The TBAB concentration of CO_2+N_2+TBAB hydrates may be very close to that of TBAB aqueous solution as TBAB hydrate was at congruent composition at w_{TBAB}=0.40 [30,31]. Therefore at w_{TBAB} <0.40, w_{TBAB} decreased as the hydrate crystal grew. The reason that the CO_2+N_2+TBAB hydrates did not cover the gas/liquid interface could be because of the shortage of TBAB around the gas/liquid interface due to the uptake of TBAB from the aqueous solution into hydrates.

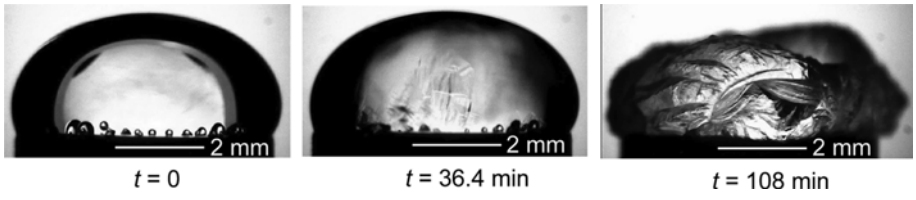

Fig. 3. Sequential images of CO_2+N_2+TBAB hydrates at w_{TBAB}=0.40, P=4.7 MPa, ΔT_{sub}=4.0 K.

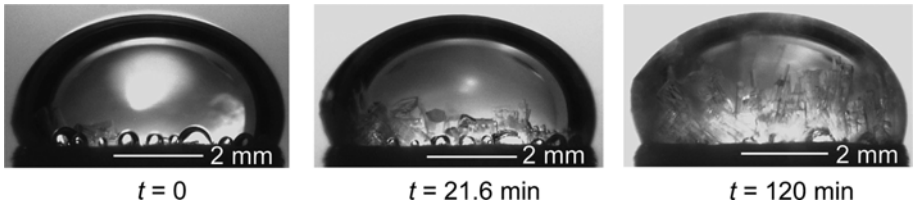

Fig. 4. Sequential images of CO_2+N_2+TBAB hydrates at w_{TBAB}=0.10, P=4.7 MPa, ΔT_{sub}=4.0 K.

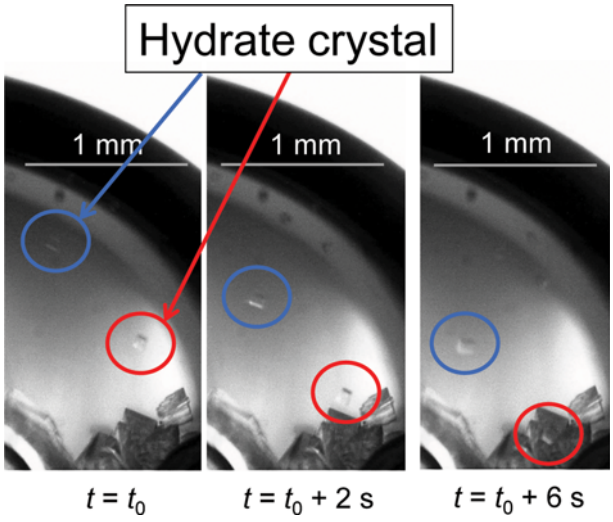

Fig. 5. Sequential images of falling hydrate crystals from interface at w_{TBAB}=0.10, P=2.3 MPa, ΔT_{sub}=6.0 K.

Sequential images of the hydrate crystals from gas/liquid interface falling into liquid phase are shown in Fig. 5. The nucleation of CO_2+N_2+TBAB hydrate was observed at a random point on the TBAB droplet surface. Hydrates are known to preferentially grow at the gas/liquid interface at first [32,33]. In contrast, CO_2+N_2+TBAB hydrates grew in the liquid phase first. The growth of hydrate within the liquid phase would be ascribed to the decrease in surface tension. Previous studies reported that the surface tension in CO_2+water [34] and CO_2+TBAB aqueous solution system [35] was increased with decreasing CO_2 partial pressure, and surface tension in N_2+water system did not significantly depend on the pressure [36]. In this study, CO_2 partial pressure was 0.46 MPa at the total pressure of 2.3 MPa, and 0.94 MPa at the total pressure of 4.7 MPa. The surface tension in this study would be higher than that in the previous study (CO_2+TBAB system at 2.3 MPa) [25] as the CO_2 partial pressure is lower. However, the addition of TBAB resulted in the hydrate crystals to be more wettable with liquid compared to the general water+gas systems. The hydrate crystals

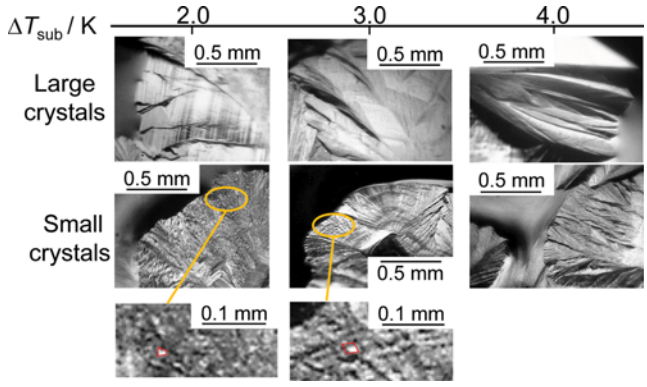

Fig. 7. Classification of the morphology of CO_2+N_2+TBAB hydrates by ΔT_{sub}.

that initially formed at CO_2+N_2 gas/TBAB aqueous solution interface were wetted and fell into TBAB aqueous solution. Therefore, it macroscopically appeared that the crystals started to grow from the liquid phase.

Fig. 6 shows sequential images of CO_2+N_2+TBAB hydrates formed at the droplet surface for w_{TBAB}=0.40. We defined the photographed time of the upper right image as t_0. The elapsed time is shown below each image. Two types of different polygonal-shaped crystals of the size were clearly observed. These crystals would have resulted from the difference in crystal structure and hydration number. Hereafter, we will call the two polygonal-shaped crystals as large crystals and small crystals. Both large and small crystals were observed at all ΔT_{sub} and pressure conditions in CO_2+N_2+TBAB system. We classified these two types of crystals by ΔT_{sub} as shown in Fig. 7. The pressure dependence of the crystal morphology was not confirmed. As for the crystal size, the large crystals length of the shortest side was 0.09 mm-0.13 mm, and the length of the longest side was less than 0.77 mm. On the other hand, small crystals had the following sizes; the shortest side was less than 0.02 mm, and the longest side was 0.07 mm. As mentioned in the introduction, the step-shaped crystals and polygonal-shaped crystals were previously observed, which had sizes of 0.14 mm×0.38 mm and

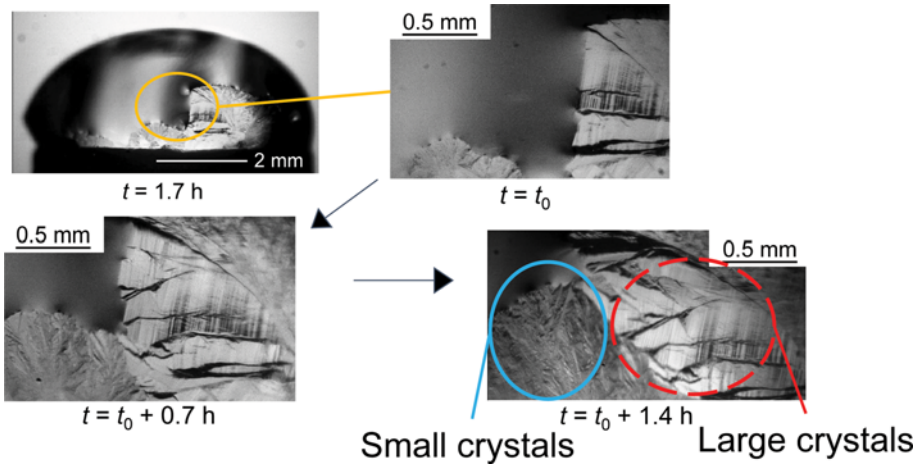

Fig. 6. Sequential images of CO_2+N_2+TBAB hydrates formed at gas/liquid interface at w_{TBAB}=0.40, P=4.77 MPa, ΔT_{sub}=2.0 K.

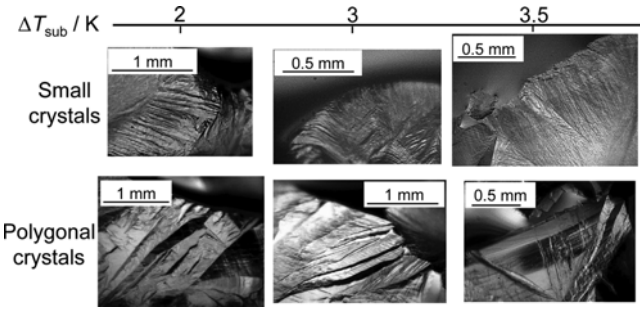

Fig. 8. Classification of the morphology of N_2+TBAB hydrates by ΔT_{sub}.

0.05 mm×0.50 mm, respectively in CO_2+TBAB system [25]. Fig. 8 shows that the observation of N_2+TBAB hydrate arranged by ΔT_{sub}. Two types of crystals were observed. One was polygonal-shaped crystals of which the length of the shortest side was 0.17 mm-0.26 mm, and the length of the longest side was 0.56 mm-1.78 mm. The other was small crystals similar to CO_2+N_2+TBAB hydrate of which the length of the shortest side was less than 0.03 mm, and the length of 0.17 mm-0.68 mm. The small crystals that formed in CO_2+N_2+TBAB systems were not observed in CO_2+TBAB systems, but were observed in N_2+TBAB system. It is then inferred that the uptake of N_2 into hydrates would have resulted in the formations of small crystals in CO_2+N_2+TBAB systems.

From the observation of results of crystal morphology, as the ratio of an area that the two types of crystals grew at the gas/liquid interface varied according to ΔT_{sub}. We approximated the curved surface of the droplet by plane and measured the area occupied by large crystals in the images and calculated the mean and standard deviation by measuring the ratio of the area that large crystals occupied as shown in Fig. 9. Note that this quantitative comparison is just an approximation because the area does not indicate the amount. Therefore, the measurement was not completely accurate, but that was utilized for a brief trend of crystal morphology changes. The ratio of the area occupied by large crystals was 7±5% at ΔT_{sub}= 2.0 K, 76±13% at ΔT_{sub}=3.0 K, 92±7% at ΔT_{sub}=4.0 K (mean is taken from more than nine samples). Therefore, we may argue that increase in the ΔT_{sub}, the increase in the ratio of the area that the large crystals occupied.

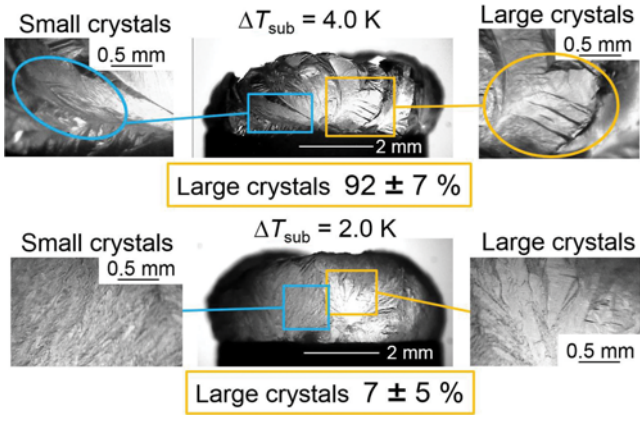

Fig. 9. The rate of area that large crystals occupied at gas/liquid interface.

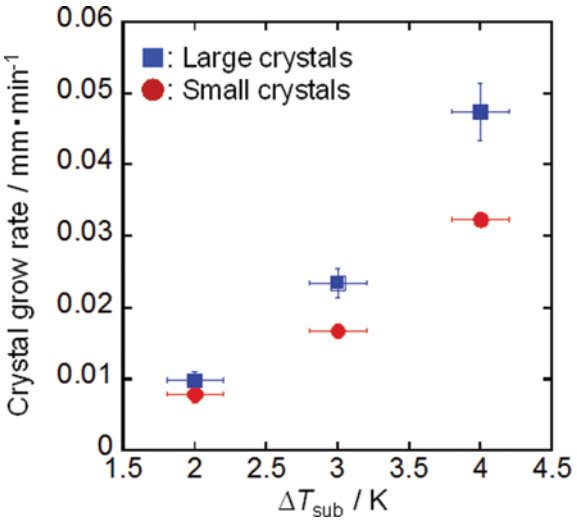

Fig. 10. Crystal growth rate of large crystals and small crystals which depend on ΔT_{sub}.

Lateral crystal growth rate of large crystals and small crystals is plotted in Fig. 10. As ΔT_{sub} increased, the lateral growth rate of large crystals also increased. However, the physical mechanism causing the difference in morphology cannot yet be clearly understood from the present experiments, and certainly a focus is necessary of future hydrate crystal morphology research.

CONCLUSION

Crystal growth behavior and crystal morphology of CO_2+N_2+TBAB ionic semiclathrate hydrate formed at the interface between CO_2+N_2 gas and TBAB aqueous solution were visually observed. The hydrate crystals were initially observed to grow within the TBAB aqueous solution. It was then followed by the lateral growth at the gas/liquid interface only at w_{TBAB}=0.40. CO_2+N_2+TBAB hydrates did not cover the gas/liquid interface at w_{TBAB}=0.10 due to the low TBAB concentration around the gas/liquid interface. It was observed that the hydrate crystals which initially formed at gas/liquid interface were wetted by the TBAB aqueous solution and fell into the solution.

As for the crystal morphology, two types of different polygonal-shaped crystals of the size were observed: large crystals and small crystals. The growth of large crystals was dominant at increased ΔT_{sub}. The physical mechanism causing the difference in morphology may be associated with polymorphism, but cannot yet be clearly defined from the present experiments. Therefore, understanding of the mechanism entrusts future hydrate crystallography research.

ACKNOWLEDGEMENT

This study was supported by a Keirin-racing-based research-promotion fund from the JKA Foundation and by JSPS KAKENHI Grant Number 25289045.

REFERENCES

1. IPCC. Climate Change 2014, *Mitigation of climate change, Contribution of Working Group III to the Fifth Assessment Report of the Intergovernmental Panel on Climate Change*., Cambridge University Press, Cambridge (2014).
2. S.-P. Kang and H. Lee, *Environ. Sci. Technol.*, **34**, 4397 (2000).
3. Y. H. Mori, *J. Chem. Ind. Eng.*, **54**, 1 (2003).
4. M. Aifaa, T. Kodama and R. Ohmura, *Cryst. Growth Des.*, **15**, 559 (2015).
5. H. Lee, J. W. Lee, D. Y. Kim, J. Park, Y.-T. Seo, H. Zeng, I. L. Moudrakovski, C. I. Ratcliffe and J. A. Ripmeester, *Nature.*, **434**, 743 (2005).
6. K. Shin, Y. Kim, T. A. Strobel, P. S. R. Prasad, T. Sugahara, H. Lee, E. D. Sloan, A. K. Sum and C. A. Koh, *J. Phys. Chem. A*, **113**, 6415 (2009).
7. P. G. Brewer, G. Friederich, E. T. Peltzer and F. M. Orr, Jr. *Science*, **284**, 943 (1999).
8. R. Ohmura and Y. H. Mori, *Environ. Sci. Technol.*, **32**, 1120 (1998).
9. B. Tohidi, J. Yang, M. Salehabadi, R. Anderson and A. Chapoy, *Environ. Sci. Technol.*, **44**, 1509 (2010).
10. T. Ogawa, T. Ito, K. Watanabe, K. Tahara, R. Hiraoka, J. Ochiai, R. Ohmura and Y. H. Mori, *Appl. Therm. Eng.*, **26**, 2157 (2006).
11. Y. Park, D.-Y. Kim, J.-W. Lee, D.-G. Huh, K.-P. Park, J. Lee and H. Lee, *Natl. Acad. Sci. U.S.A.*, **34**, 12690 (2006).
12. Y.-T. Seo, I. L. Moudrakovski, J. A. Ripmeester, J.-W. Lee and H. Lee, *Environ. Sci. Technol.*, **39**, 2315 (2005).
13. R. B. Bird, W. E. Stewart and E. N. Lightfoot, *Transport Phenomena*, 2nd Ed., Wiley, Hoboken, NJ, 196 (2006).
14. M. Darbouret, M. Cournil and J. M. Herri, *Int. J. Refrig.*, **28**, 663 (2005).
15. D. Zhong and P. Englezos, *Energy Fuels*, **26**, 2098 (2012).
16. D. L. Zhong, Y. Ye and C. Yang, *J. Chem. Eng. Data*, **56**, 2899 (2011).
17. P. Babu, W. I. Chin, R. Kumar and P. Linga, *Ind. Eng. Chem. Res.*, **53**, 4878 (2014).
18. S. Li, S. Fan, J. Wang, X. Lang and D. Liang, *J. Nat. Gas Chem.*, **18**, 15 (2009).
19. V. Belandria, A. H. Mohammadi and D. Richon, *Chem. Eng. Sci.*, **84**, 40 (2012).
20. Y. Lee, S. Lee, J. Lee and Y. Seo, *Chem. Eng. J.*, **246**, 20 (2014).
21. J. Deschamps and D. Dalmazzone, *J. Therm. Anal. Calorim.*, **98**, 113 (2009).
22. H. Oyama, W. Shimada, T. Ebinuma, Y. Kamata, S. Takeya, T. Uchida, J. Nagao and H. Narita, *Fluid Phase Equilib.*, **234**, 131 (2005).
23. H. P. Veluswamy, T. Yang and P. Linga, *Cryst. Growth Des.*, **14**, 1950 (2014).
24. S. Koyanagi and R. Ohmura, *Cryst. Growth Des.*, **13**, 2087 (2013).
25. H. Akiba, H. Ueno and R. Ohmura, *Cryst. Growth Des.*, **15**, 3963 (2015).
26. A. Chapoy, R. Anderson and B. Tohidi, *J. Am. Chem. Soc.*, **129**, 746 (2007).
27. M. Arjmandi, A. Chapoy and B. Tohidi, *J. Chem. Eng. Data*, **52**, 2153 (2007).
28. P. Meysel, L. Oellrich, P. R. Bishnoi and M. A. Clarke, *The J. Chem. Thermodyn.*, **43**, 1475 (2011).
29. S. Kim and Y. Seo, *Appl. Energy*, **154**, 987 (2015).
30. S. Muromachi, K. A. Udachin, K. Shin, S. Alavi, I. L. Moudrakovski, R. Ohmura and J. A. Ripmeester, *Chem. Commun.*, **50**, 11476 (2014).
31. K. Sato, H. Tokutomi and R. Ohmura, *Fluid Phase Equilib.*, **337**, 115 (2013).
32. R. Tanaka, R. Sakemoto and R. Ohmura, *Cryst. Growth Des.*, **9**, 2529 (2009).
33. K. Saito, M. Kishimoto, R. Tanaka and R. Ohmura, *Cryst. Growth Des.*, **11**, 295 (2011).
34. A. Georgiadis, G. Maitland, J. P. M. Trusler and A. Bismarck, *J. Chem. Eng. Data*, **55**, 4168 (2010).
35. H. Akiba and R. Ohmura, *J. Chem. Thermodyn.*, **92**, 72 (2015).
36. W. Yan, G. Y. Zhao, G. J. Chen and T. M. Guo, *J. Chem. Eng. Data*, **46**, 1544 (2001).